

Chapter 2

Experimental Environment

The measurement presented in this thesis is based on a data set collected between April 2002 and May 2008 with the DØ experiment at the Fermilab. The collected data set corresponds to an integrated luminosity of 2.8 fb^{-1} . Besides the DØ detector, a second omni-purpose detector has been built at the Tevatron to study proton–antiproton collisions, CDF. During the so-called Run I period of the Tevatron accelerator (1991–1996), both CDF and DØ reported the discovery of the top quark in 1995.

The following chapter gives an overview of the experimental setup of this analysis. After a short description of the accelerator complex in [Sect. 2.1](#), [Sect. 2.2](#) describes the different components of the DØ detector, as well as the trigger system and the data acquisition.

2.1 The Tevatron Accelerator Complex

The Tevatron is a proton–antiproton collider with a circumference of 6.3 km and a center-of-mass energy of $\sqrt{s} = 1.96 \text{ TeV}$. Up to the start of the LHC in 2009, it is the most energetic accelerator in the world, and the only place on Earth where top quarks can be produced directly. In the Run I period of the Tevatron, the center-of-mass energy was $\sqrt{s} = 1.8 \text{ TeV}$, and both CDF and DØ collected an integrated luminosity of around 100 pb^{-1} . Starting in 1996, the accelerator was upgraded to achieve a center-of-mass energy of 1.96 TeV and a higher instantaneous luminosity. Nowadays peak luminosities are generally around $300 \mu\text{b}^{-1} \text{ s}^{-1}$.

Figure 2.1 shows the accelerator complex at the Fermilab, where the Tevatron itself is only the last one in a chain of seven accelerators. The most important parts of this complex are the following:

- *Cockroft–Walton preaccelerator* Hydrogen gas is ionized to create H^+ ions which are then accelerated to 750 keV.

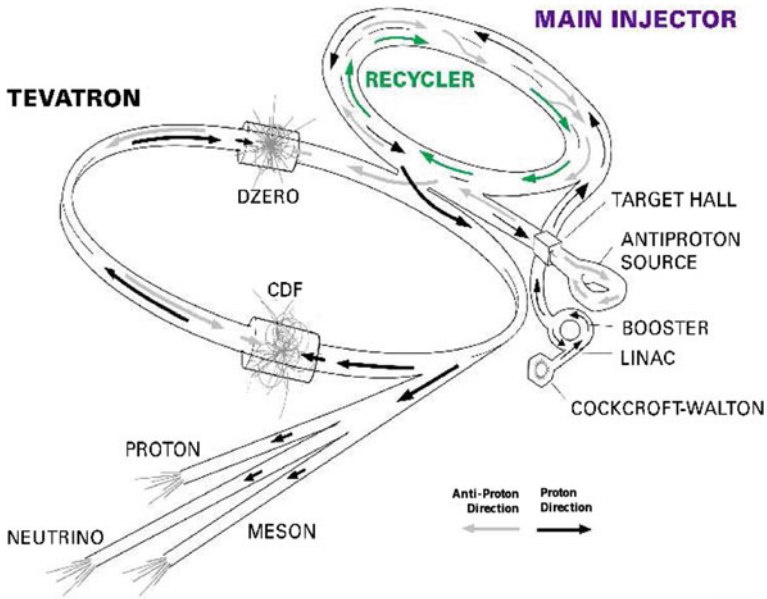


Fig. 2.1 Schematic overview of the Fermilab accelerator complex [1]

- *Linear accelerator (Linac)* The Linac is 150 m long and accelerates the H^- ions to an energy of 400 MeV.
- *Booster* The Booster is the first synchrotron in the accelerator chain and has a circumference of about 475 m. A carbon foil strips the electrons from the H^- ions at injection and leaves bare protons. The intensity of the proton beam is increased by injecting additional H^- ions into the same orbit as the circulating ones. The protons are accelerated from 400 MeV to 8 GeV by a series of RF cavities.
- *Main Injector* The Main Injector is a synchrotron with a circumference of 3 km and two important key tasks. First of all, it accelerates protons from 8 to 120 GeV to produce antiprotons by directing the protons to a nickel target in the fixed target hall. Secondly, it accelerates both protons from the Booster and antiprotons from the Recycler to 150 GeV to inject them into the Tevatron.
- *Accumulator* In the Accumulator, a pulsed magnet separates the antiprotons from other particles and a lithium current lens is used to focus the beam. Additionally, the beam width is reduced by the so-called stochastic cooling. Here, pickup sensors sample the average transverse excursion for portions of each bunch, so that kicker magnets can apply correction forces to damp the antiproton beam on average.
- *Recycler* The Recycler is located in the same ring as the Main Injector. It recycles the antiprotons when the beam becomes poor after many collisions and integrates the cooled antiprotons in a stack.

- *Tevatron* In a last step, the Tevatron accelerates protons and antiprotons in opposite directions from 150 to 980 GeV. Superconducting magnets with a field of 4.2 T are used to keep the 36 bunches of protons and antiprotons on track. Each proton bunch contains 3×10^{11} particles, each antiproton bunch, 3×10^{10} . Finally they are brought to collision where the CDF and DØ detectors are built. The distance in time between two bunch crossings is 396 ns.

More information on the accelerator complex can be found in the design report [2].

2.2 The DØ Experiment

The DØ detector shown in Fig. 2.2 is one of the two omni-purpose detectors built at the Tevatron accelerator to study proton–antiproton collisions. It consists of three major subsystems: a tracking detector for vertex identification and momentum measurements, a uranium–liquid argon calorimeter to measure the energy of electromagnetic and hadronic showers, and a muon spectrometer to detect and measure muon momenta. After a short introduction of the coordinate system used at the DØ experiment, the most important aspects of the different subcomponents of the detector are discussed. A detailed description of the DØ detector is provided by the DØ collaboration [3].

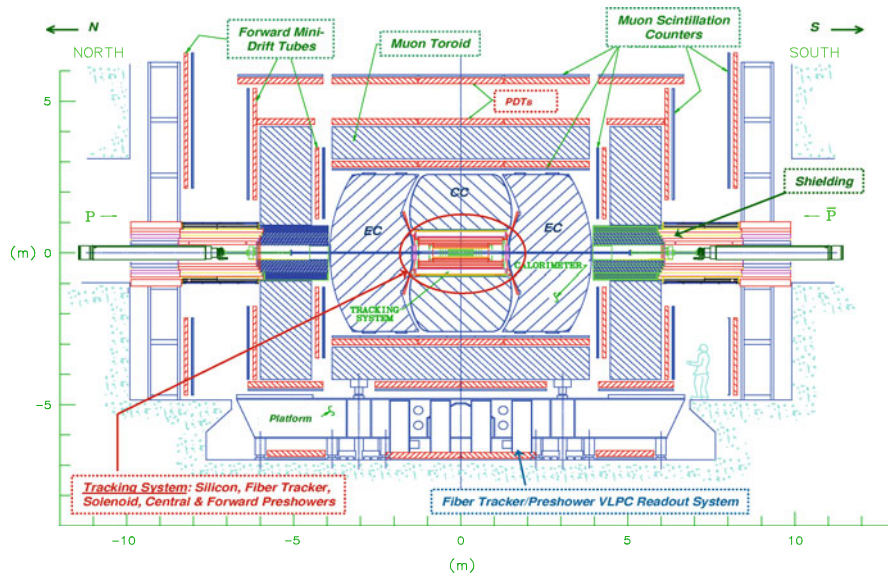


Fig. 2.2 Schematic profile of the DØ detector [4]

2.2.1 The Coordinate System

The right-handed coordinate system of the DØ detector is chosen such that its origin is at the nominal collision point. The x axis points to the center of the Tevatron ring, the y axis upwards, and the z axis along the direction of the proton beam. Alternatively to the polar angle θ , the pseudorapidity η is used. It is given by

$$\eta = -\ln\left(\tan\frac{\theta}{2}\right). \quad (2.1)$$

Consequently, the spatial separation between two particles is quantified in terms of

$$\Delta R = \sqrt{\Delta\eta^2 + \Delta\phi^2}, \quad (2.2)$$

where $\Delta\phi$ denotes the azimuthal angle.

2.2.2 The Tracking System

The barrel-shaped tracking system shown in Fig. 2.3 consists of the silicon microstrip tracker (SMT) and the central fiber tracker (CFT) within a solenoidal magnetic field of 2 T. First, it is designed to measure the momentum of charged particles via the curvature of their track within $|\eta| < 3$. Secondly, it separates electrons from pions, and detects secondary vertices for b quark identification. The primary interaction vertex resolution is about $35\ \mu\text{m}$ and the momentum resolution in the central region about $\Delta p_T/p_T = 17\%$ for $p_T = 100\ \text{GeV}$ [5].

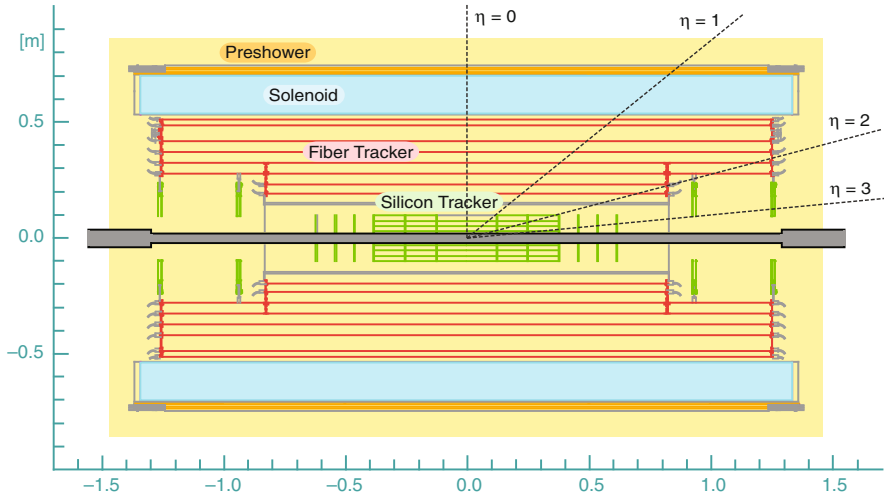


Fig. 2.3 Schematic drawing of the central tracking system [6]

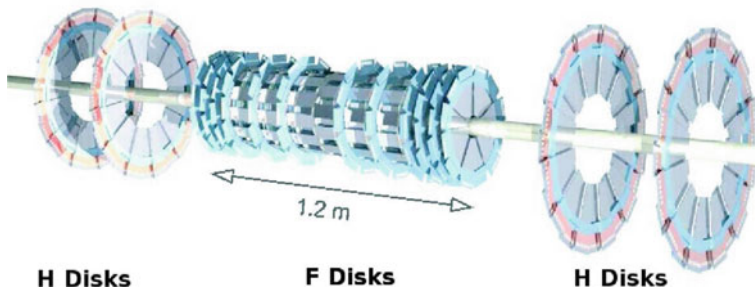


Fig. 2.4 Arrangement of the disks and barrels in the SMT [7]

2.2.2.1 Silicon Microstrip Tracker

The SMT shown in Fig. 2.4 uses reverse biased p–n junctions to detect particle tracks. It covers a range up to $|\eta| < 3$. Any passing charged particle causes ionization and electron-hole pairs are produced in the semiconductor. Reading out the charge deposition separately on every strip, the position of the particle can be measured with excellent resolution.

The SMT is composed of three subdetectors: the central barrels, the F disks and the H disks. The central barrels are made out of 5 (before 2005 only four) double layers of silicon detectors, and the 12 F disks, out of 12 double-sided wedge detectors. Six F disks are located in between the barrels with one attached to each end of the barrel detector, and six F disks, in a small distance from either end of the barrel detector. The two large-diameter H disks consisting of 24 wedges are mounted about 1 m from the interaction point. Each of the 24 wedges is constructed out of two back-to-back single-sided wedges. The barrels are used to measure the r – ϕ component of a particle, while the disks can measure both r – ϕ and r – z . The SMT provides a hit resolution of around 10 μm .

2.2.2.2 Central Fiber Tracker

The CFT surrounds the SMT with eight cylindrical layers of two fiber doublets, and provides a coverage up to $|\eta| < 1.6$. When a charged particle penetrates one of the fibers, the scintillator emits light via a rapid fluorescence decay. To increase the mean free path length of the light in the fiber, the fiber absorbs well at $\lambda = 340$ nm and emits at $\lambda = 530$ nm. The light is finally collected on one side of the fiber by a wave guide carrying the scintillation light to visible light photon counters for readout.

For each cylindrical layer, there is one doublet layer of fibers oriented parallel to the beam axis and one doublet layer enclosing an angle of ϕ with the beam axis, where ϕ alternately is $+3^\circ$ and -3° starting with $+3^\circ$ from the innermost layer. To fill all gaps, each doublet is made of two layers with an offset of half a fiber width to each other. The CFT has a hit resolution of about 100 μm .

2.2.2.3 The Preshower Detectors

Outside the solenoid magnet, two additional tracking detectors are located: the central and the forward preshower detectors (CPS and FPS). The CPS is mounted on the solenoid and covers the range of $|\eta| < 1.3$, the FPS is on the inner surface of the end-calorimeter cryostat and covers the range of $1.5 < |\eta| < 2.5$. The lead absorbers of the preshower detectors convert electromagnetic particles (electrons and photons) into showers, and the shower energy is measured by several layers of scintillator strips. Besides the precise measurement of tracks in addition to the central tracker, the preshower detectors are used to correct the electromagnetic energy measurement of the central and the end calorimeters for losses in the solenoid and upstream material. In addition, they help to identify electrons and reject background.

2.2.3 The Calorimeter

The calorimeter shown in Fig. 2.5 consists of three parts embedded in three separate cryostats with a temperature of 90 K: the central calorimeter (CC) covering a range up to $|\eta| = 1$, and two end-cap calorimeters, one south of the interaction point (ECS) and one north (ECN) extending the covered range up to $|\eta| = 4$.

The main purpose of the calorimeter is the measurement of the energy of photons, electrons, and jets by inducing them to produce electromagnetic and hadronic showers. In addition, it helps to identify photons, electrons, jets, and muons, and it is used to measure the transverse energy balance in events.

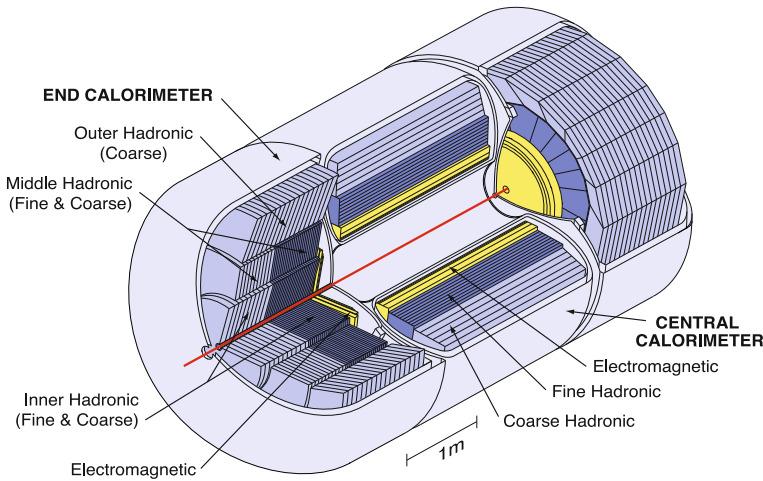


Fig. 2.5 Schematic drawing of the Run II DØ calorimeter [6]

Each of the three calorimeters contains an electromagnetic (EM) section closest to the interaction region followed by fine (FH) and coarse hadronic (CH) sections. The active medium of the calorimeter is always liquid argon, whereas the absorber in the electromagnetic section is depleted uranium, in the fine hadronic modules, uranium–niobium (2%) alloy, and in the coarse hadronic modules, copper (CC) or stainless steel (EC). The active medium is needed to sample and measure the energy of the shower through ionization, while the absorber causes the particles to shower.

The so-called inter-cryostat detector (ICD) is situated in between the CC and EC to compensate for the dead region between the cryostats. It consists of one layer of scintillating tiles mounted on the cryostat and is read out by photo-tubes that are connected by wavelength-shifting fibers.

The transverse size of the readout cells are comparable to the one of showers: 1–2 cm for electromagnetic showers and about 10 cm for hadronic showers. The granularity in η and ϕ is 0.1×0.1 . The third layer of the EM modules, located at the electromagnetic-shower maximum, is segmented twice as finely to allow a more precise location of the electromagnetic-shower centroids.

The energy resolution of electromagnetic and hadronic objects in the calorimeter can be parameterized as

$$\frac{\Delta E}{E} = \sqrt{\frac{S^2}{E(\text{GeV})} + \frac{N^2}{E^2(\text{GeV})^2}} + C^2, \quad (2.3)$$

where S describes fluctuations in the energy deposition, N , instrumental effects like uranium noise, and C , uncertainties in the calibration. These parameters are measured from data and listed in Table 2.1.

2.2.4 The Muon Spectrometer

The muon system surrounds all other detector components and consists of two parts: the central muon system covering the region up to $|\eta| = 1$, and the forward muon system covering the region of $1 < |\eta| < 2$. A toroidal magnet of 1.8 T allows a separate measurement of the muon momentum in the muon spectrometer. Gas filled tubes are used to collect and to measure the ionization created by the passing muons.

For a central muon with a transverse momentum of 40 GeV, the momentum resolution is measured to be $\Delta p_T/p_T = (9.6 \pm 0.3)\%$ [10]. The resolution is

Table 2.1 Parameters for the energy resolution in the calorimeter [8, 9]

| | C | $S(\sqrt{\text{GeV}})$ | $N(\text{GeV})$ |
|------------------|-------|------------------------|-----------------|
| Electron, photon | 0.041 | 0.15 | 0.29 |
| Jet | 0.036 | 1.05 | 2.13 |

limited by multiple scattering at low momentum and the individual hit resolution at high momentum. Nevertheless, it allows a cleaner matching with the central tracks, rejection of π and K in-flight decays, and yields an improved momentum resolution at high muon momenta.

2.2.4.1 The Central Muon System

The central muon system consists of three layers A, B, and C of proportional drift tubes (PDTs), see Fig. 2.6. While layer A is located between the cryostat and the toroidal magnet, layer B and C are outside the toroidal magnet. Since the drift time of the PDTs (750 ns) is longer than the bunch crossing time of the Tevatron, two additional layers of scintillators shown in Fig. 2.7 are used to trigger muon events: the A- ϕ counters between the calorimeter and layer A, and the cosmic caps mounted outside layer C. The A- ϕ counters are also used to reject cosmic muons and scattered particles from the calorimeter, the cosmic caps are used to reject cosmic muons. Due to the support structure of the DØ detector, the bottom part of the detector is only partly covered with scintillator counters. The resolution of the PDTs is about 1 mm.

2.2.4.2 The Forward Muon System

The forward muon system consists of three layers A, B, and C of mini drift tubes (MDTs) and scintillator counters, see Fig. 2.6. The MDTs have been newly built for Run II. Here, also layer A is between the cryostat and the toroidal magnet, while layer B and C are outside the magnet. Though the drift time of the MDTs is

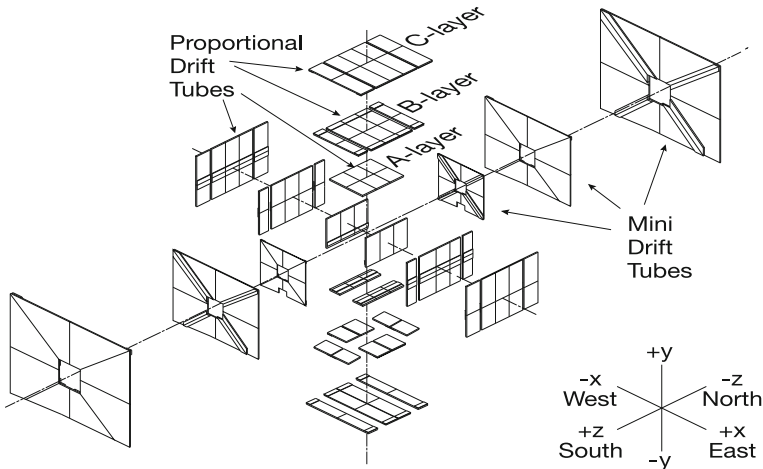


Fig. 2.6 Arrangement of the PDTs and MDTs in the muon system [3]

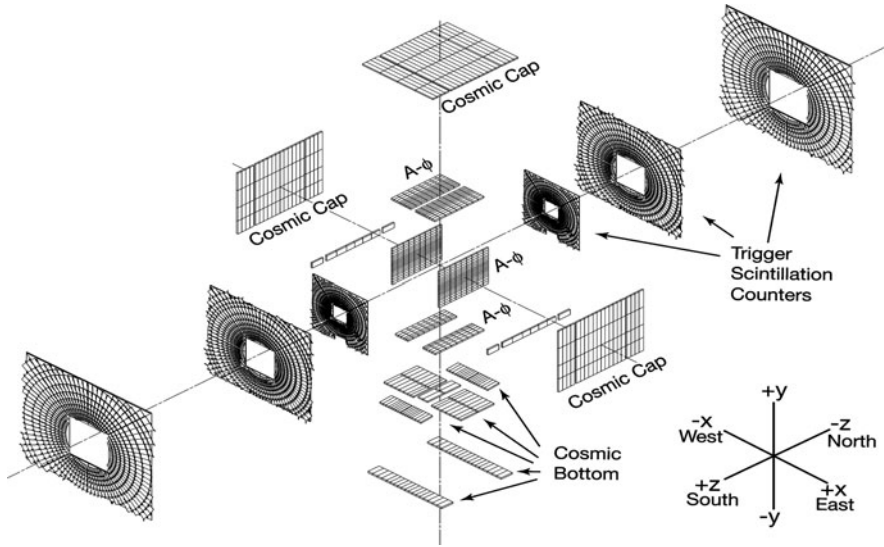


Fig. 2.7 Arrangement of the scintillation detectors in the muon system [3]

only 60 ns, scintillation counters are also used to trigger muon events and to reject cosmic muons and other sources of background. The forward muon system has additional shielding around the beam pipe to reduce trigger rates and the aging of the detector by beam halo. The resolution of the MDTs is about 0.7 mm.

2.2.5 The Luminosity Monitors

The instantaneous luminosity is given by

$$\mathcal{L} = \frac{1}{\sigma_{pp}^{\text{eff}}} \frac{dN_{p\bar{p}}}{dt}, \quad (2.4)$$

where σ_{pp}^{eff} denotes the effective inelastic $p\bar{p}$ cross section measured by the luminosity monitors taking detector acceptance and efficiency into account. The luminosity monitors are two hodoscopes built from plastic scintillators mounted on the cryostats of the end-cap calorimeters. They cover a pseudorapidity of $2.7 < |\eta| < 4.4$. In order to distinguish between $p\bar{p}$ interactions and beam halo, the z coordinate of the interaction vertex is calculated from the difference in time-of-flight between the two luminosity monitors. Particles from inelastic $p\bar{p}$ collisions have a smaller time-of-flight difference than particles from the beam halo. The overall estimated error on the luminosity is 6.5%.

The integrated luminosity is calculated in so-called luminosity blocks. Each luminosity block is indexed by a luminosity block number. After each run or store

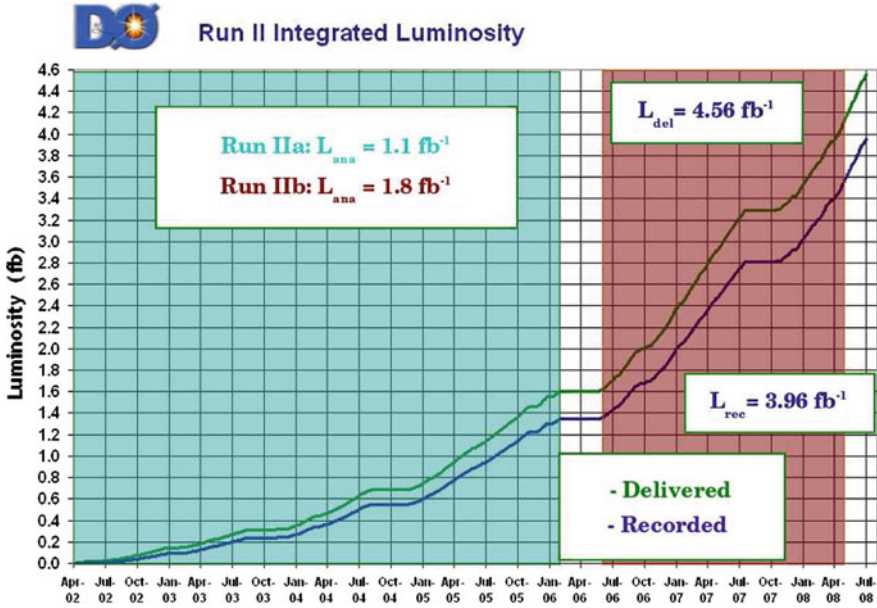


Fig. 2.8 Integrated luminosity delivered to and recorded by the DØ experiment in Run II until July 2008

transition the number monotonically increases. The time period is chosen such that for each luminosity block the integrated luminosity is about the same.

Figure 2.8 shows the integrated luminosity delivered to and recorded by the DØ experiment. The average data taking efficiency is about 89% and up to now, 4 fb^{-1} are stored on tape by the DØ experiment. The measurement presented in this analysis uses the full reconstructed data set of 2.8 fb^{-1} . The data set is split in two periods, Run IIa from April 2002 to February 2006 with 1.1 fb^{-1} , and Run IIb from June 2006 to May 2008 with 1.7 fb^{-1} . It has to be noticed that the Run I data set is not included as the center-of-mass energy was increased between Run I and Run II, and a measurement of the charged track momentum was not possible during Run I.

2.2.6 The Trigger System and Data Acquisition

The trigger system is designed to reduce the event rate delivered by the Tevatron to an event rate that can be written to tape and is practical to analyze. Most of the events produced in $p\bar{p}$ collisions are multijet events, while the production cross section of massive bosons, top quarks, or particles beyond the Standard Model is extremely small. To select these events, the trigger system is designed to select

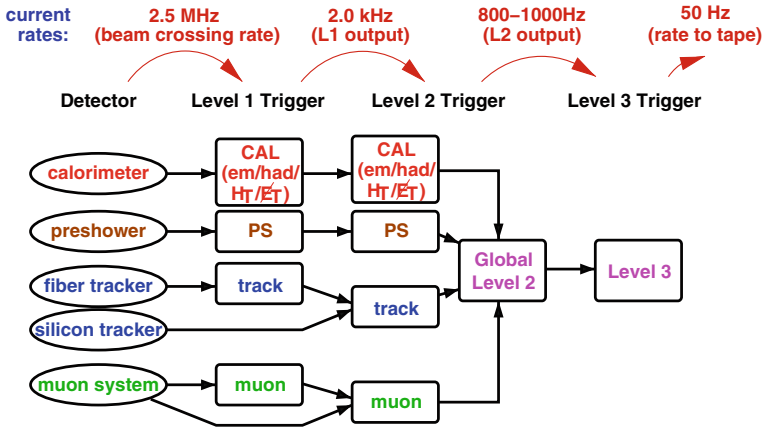


Fig. 2.9 Outline of the DØ trigger system

events with high transverse momentum jets or leptons. The DØ trigger system consists of three levels: Level 1 (L1), a pure hardware trigger using electronic signals from the detector, Level 2 (L2), using both electronic signals and reconstructed physics objects, and Level 3 (L3), a pure software trigger, using only reconstructed objects. A diagram of the trigger system is shown in Fig. 2.9.

2.2.6.1 Level 1 Trigger

The L1 trigger reduces the event rate from 2.5 MHz to about 2 kHz in about 4.2 μ s. It consists of a luminosity trigger, a calorimeter trigger, a central-track trigger and a muon-system trigger. The luminosity system provides indication that a collision occurred, and the tracking system reconstructs tracks and stores seed track candidates to be used by other trigger units. The calorimeter performs a fast summation of electromagnetic and hadronic towers to look for towers that exceed a certain threshold. The muon triggers require coincidence between signals in layer A and either B or C.

2.2.6.2 Level 2 Trigger

The L2 trigger reduces the event rate to 1 kHz and takes about 100 μ s to make a decision. The system consists of two stages. In the preprocessor stage, the information from the different subsystems is used to reconstruct physics objects; in the global stage, the information across the subsystems is used to build physics objects. The preprocessor stage consists of the L2 calorimeter trigger, the L2 preshower trigger, the L2 muon-system trigger, the L2 SMT trigger, and the L2 central-track trigger.

2.2.6.3 Level 3 Trigger

The L3 trigger finally reduces the rate to about 50 Hz. This software trigger uses a simplified event reconstruction algorithm and is fully based on reconstructed physics objects.

2.2.6.4 The Data Acquisition System

The transport of the selected data events from the readout crates to the farm nodes is done with the data acquisition (DAQ) system. The triggering and the data acquisition are controlled by a coordination program called COOR. The readout of the luminosity monitors is done with a standalone DAQ system.

References

1. The Tevatron accelerator division. <http://www-bd.fnal.gov/public/relativity.html>.
2. The Tevatron accelerator division (1988) Proton–antiproton collider upgrade, FERMILAB-DESIGN-1988-01
3. Abazov VM et al (DØ collaboration) (2006) The upgraded DØ detector. Nucl Instrum Meth A 338:463
4. The DØ collaboration. <http://www-d0.fnal.gov/Run2Physics/displays/presentations/#gallery>
5. Ellison J (2001) The DØ detector upgrade and physics program. DØ note 3830
6. The DØ collaboration. http://www-d0.fnal.gov/Run2Physics/top/top_public_web_pages/top_dzero_detector.html
7. The DØ collaboration. <http://www-d0.fnal.gov/Run2Physics/WWW/drawings.htm>
8. Chaplin D et al (2005) Measurement of $Z \rightarrow ee$ and $W \rightarrow ev$ production cross sections using one tight electron. DØ note 4897
9. Royon C et al (2007) Jet pT resolution using v7.1 JES for p17 data. DØ note 5381
10. Calfayan P et al (2006) Muon identification certification for p17 data. DØ note 5157

Measurement of the Top Quark Mass in the Dilepton
Final State Using the Matrix Element Method

Grohsjean, A.

2010, X, 150 p. 73 illus., 25 illus. in color., Hardcover

ISBN: 978-3-642-14069-3